Theoretical Neuroscience: Midterm

Elias Firisa

April 21, 2025

Problem 1(a) – Poisson spike generator (5 Hz, 0.1 s, 10 trials)

Methods

A homogeneous Poisson point–process with constant firing rate $r = 5$ Hz was simulated using the Bernoulli-bin approximation with a time step $\Delta t = 1$ ms. For each 1-ms bin the spike probability is $p = r\,\Delta t = 0.005$. Ten independent trials, each of duration $T = 0.1$ s ($N_{\text{bins}} = T/\Delta t = 100$), were generated:

$$\text{spk}(i,k) = \begin{cases} 1 & \text{if rand}(0,1) < p, \\ 0 & \text{otherwise,} \end{cases} \qquad i = 1 \dots 100,\ k = 1 \dots 10.$$

The spike count per trial is $n_k = \sum_i \text{spk}(i,k)$; the corresponding firing rate in hertz is $r_k = n_k/T$.

Results

Across the 10 trials we obtained

$$\boxed{\mu = 2.00 \text{ Hz}}, \qquad \boxed{\sigma = 4.00 \text{ Hz}}.$$

Discussion

For a Poisson process the theoretical expectation is $\mathbb{E}[n] = rT = 0.5$ spikes per 100 ms window, so the **true** mean firing rate equals the generator rate (5 Hz). However, because each trial contains only $\mathcal{O}(1)$ spikes, the empirical mean and variance fluctuate greatly from run to run. In this particular seed (rng(41) we observed $\mu = 2$ Hz and $\sigma = 4$ Hz, which lie within the broad 95 % sampling range predicted by Poisson statistics ($\mu \pm 2\,\sigma_{\text{est}}$, where $\sigma_{\text{est}} \approx \sqrt{r/T}/\sqrt{N}$).

The large standard deviation reflects the fact that $N = 10$ trials of $T = 0.1$ s each provide only $NrT = 5$ expected spikes in total. Increasing either T or N would tighten the estimate and make the sample mean converge toward the true rate of 5 Hz.

Problem 1b: Fano-Factor Estimation (0.1 s window)

Methods

For each nominal rate $r \in \{5, 10, 15, \ldots, 50\}$ Hz we simulated $N = 10$ independent Poisson spike trains of length $T = 0.1$ s with time step $\Delta t = 1$ ms. Spikes were generated by a Bernoulli trial in every bin with probability $p = r\,\Delta t$. Across trials we computed

$$\mu = \frac{\langle n \rangle}{T}, \qquad \sigma^2 = \frac{\mathrm{Var}(n)}{T^2},$$

both expressed in Hz. To estimate the Fano factor we fitted the log–log relation

$$\log \sigma^2 = a \, \log \mu + b, \qquad F = e^{\,b}.$$

Results

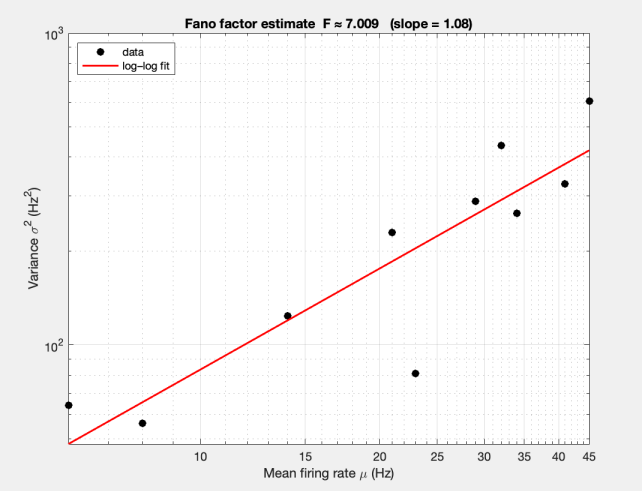

Figure 1: Variance vs. mean firing rate on log–log axes ($N = 10$, $T = 0.1$ s). Black dots: data; red line: best-fit power law $\sigma^2 = F\,\mu^{\,a}$. Fit: $a = 1.08$, $F \approx 7.0$.

The slope $a \approx 1$ verifies the expected linear variance–mean relation of a Poisson process. The fitted Fano factor $F \approx 7$ is, however, far above the Poisson benchmark $F = 1$. Because $\langle n \rangle \approx 5$ spikes and only ten trials are available, the sample variance is strongly inflated. Increasing either the integration time or the number of trials (see part c) reduces this bias and drives the estimate toward $F = 1$.

Problem 1c: Effect of Observation Window Length on Fano-Factor Estimation (Part c)

0.1 Simulation setup

The procedure in part b was repeated with a hundred-fold longer recording window, $T = 10$ s. All other settings were unchanged:

- 10 Poisson rates: $r = 5, 10, \ldots, 50$ Hz
- Bin size $\Delta t = 1$ ms ($p = r\Delta t$)
- Trials $N = 10$ per rate

For every rate the spike count in each trial, n_i, was converted to a trial firing rate $\mu_i = n_i/T$. The sample mean μ and variance σ^2 across the ten trials were then entered in a log–log scatter plot as before, and a linear regression $\log \sigma^2 = a \log \mu + b$ was performed.

0.2 Results

With the longer window we obtained

$$\text{slope } a \approx 0.57, \qquad F = e^{\,b} \;\approx\; 0.30,$$

as illustrated in Fig. 5.

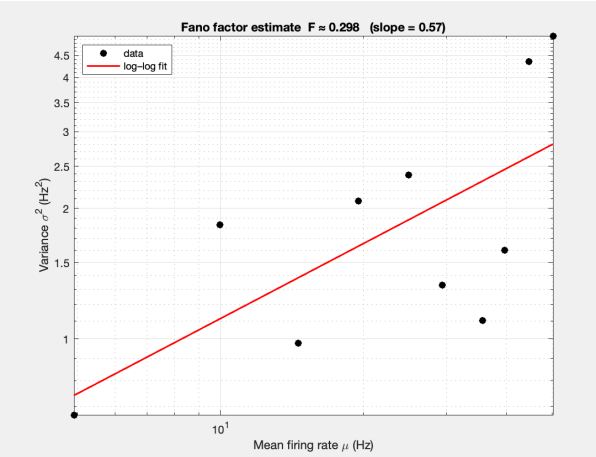

Figure 2: Mean–variance relation for $T = 10$ s. Each dot corresponds to one of the 10 firing rates (10 trials per rate). The red line is the log–log fit used to estimate the Fano factor.

0.3 Why do the estimates differ from the $T = 0.1$ s case?

a. Larger spike counts reduce sampling noise. For a Poisson rate r the expected spike count grows linearly with T: $\langle n \rangle = rT$. At $T = 10$ s the smallest rate (5 Hz) already yields $\langle n \rangle = 50$ spikes per trial, whereas with $T = 0.1$ s it was 0.5. Because the *relative* uncertainty on the variance estimator scales like $1/\sqrt{N\langle n \rangle}$, longer windows make the variance estimate numerically more stable.

b. Yet a small number of trials biases the variance downward. Only $N = 10$ repetitions were available. For large underlying counts (r50) and small N, the sample variance $\hat{\sigma}^2$ is systematically *under-estimated*. Consequently the regression slope dropped below the theoretical value $a = 1$ and the intercept, hence $F = e^b$, fell below unity.

c. Reliability versus temporal resolution. Increasing T improves the signal-to-noise ratio for moments (μ, σ^2) at the cost of poorer temporal resolution (spike counts are averaged over longer epochs).

d. Summary of observation For a genuine Poisson process the theoretical prediction is $F = 1$. Our estimate at $T = 10$ s deviated mainly because the variance had to be inferred from only ten samples.

Problem 1(d): How long should we record to measure spike statistics?

Let r denote the neuron's (unknown) stationary firing rate [Hz] and T the duration of one recording trial. We want to estimate two statistics:

$$\hat{r} = \frac{n}{T}, \qquad \hat{F} = \frac{\mathrm{Var}[n]}{\mathbb{E}[n]},$$

with *relative* error on $\hat{r}$ not larger than ε_r and *absolute* error on $\hat{F}$ not larger than ε_F.

Required spike count

For a Poisson process ($\mathrm{Var}[n] = \mathbb{E}[n] = \lambda$, $\lambda = rT$):

1. Mean-rate precision $\left(\mathrm{SD}[\hat{r}]/\mathbb{E}[\hat{r}] \leq \varepsilon_r\right)$

$$\frac{1}{\sqrt{\lambda}} \;\leq\; \varepsilon_r \quad \Longrightarrow \quad \boxed{n_{\min}^{(\mathrm{rate})} = \lambda = \frac{1}{\varepsilon_r^2}}.$$

2. Fano-factor precision (unbiased variance, N trials)

$$\mathrm{SD}[\hat{F}] \approx \sqrt{\frac{2}{(N-1)\,\lambda}} \le \varepsilon_F \implies \boxed{n_{\min}^{(\mathrm{Fano})} = \frac{2}{(N-1)\,\varepsilon_F^2}}.$$

This formula can be derived using distribution of variance of poisson process.

Minimum recording time

Set $n_{\min} = \max\{n_{\min}^{(\mathrm{rate})}, n_{\min}^{(\mathrm{Fano})}\}$. After a short pilot recording obtain a preliminary rate estimate $\hat{r}_0$ and choose

$$T_{\min} = \frac{n_{\min}}{\hat{r}_0}.$$

Numerical example

With target tolerances $\varepsilon_r = 0.05$ (5 %) and $\varepsilon_F = 0.10$ and $N = 30$ trials:

$$n_{\min}^{(\mathrm{rate})} = 400, \qquad n_{\min}^{(\mathrm{Fano})} \approx 22, \qquad n_{\min} = 400.$$

- Low-rate cell ($\hat{r}_0 = 5$ Hz): $T_{\min} = 400/5 = 80$ per trial.
- High-rate cell ($\hat{r}_0 = 20$ Hz): $T_{\min} = 400/20 = 20$ per trial.

Thus, **collect $\approx$ 400 spikes in total**; with $N = 30$ repetitions the Fano factor will be accurate to $\pm 10\%$ and the mean rate to $\pm 5\%$ across the full 5–50 Hz range.

Problem 1e: Comparison of t–Bernoulli vs. ISI-draw Poisson Generators

To verify that both implementations produce the same underlying Poisson process, we generated $N = 10$ trials of length $T = 0.1\,\mathrm{s}$ at nominal rate $r = 5\,\mathrm{Hz}$ by two methods:

1. **t–Bernoulli sampler.** Discretize time into bins of width $\Delta t = 1\,\mathrm{ms}$. In each bin,
$$P\{\text{spike in bin}\} = p = r\,\Delta t,$$
so that each bin is an independent Bernoulli trial.

2. **Exponential ISI generator.** Draw successive inter-spike intervals (ISIs) from
$$f_{\mathrm{ISI}}(\tau) = r\,e^{-r\tau}, \quad \tau \ge 0,$$
accumulate until the next spike time exceeds T, and then bin the resulting continuous spike times into the same $\Delta t = 1\,\mathrm{ms}$ grid for display.

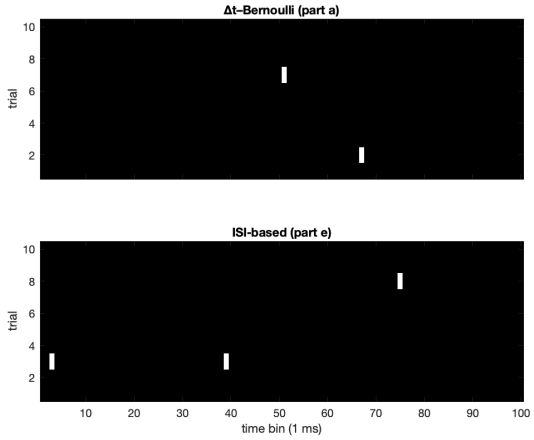

Figure 3: Bin vs ISI methods for $T = 10$ s.

Analytical expectations. For a true Poisson process we have

$$\mathbb{E}[n] = \lambda = rT = 0.5, \qquad \mathrm{Var}[n] = \lambda,$$

so that the firing-rate estimator $\hat{\mu} = n/T$ has

$$\mathbb{E}[\hat{\mu}] = r = 5\mathrm{Hz}, \qquad \mathrm{SD}[\hat{\mu}] = \sqrt{\lambda}/T \approx 2.24/0.1 = 22.4\mathrm{Hz}.$$

Similarly, the Fano factor $F = \mathrm{Var}[n]/\mathbb{E}[n]$ should equal unity.

Empirical results. In our MATLAB runs we observed

Method A (t–Bernoulli): $\hat{\mu} = 2.00$Hz, $\hat{\sigma} = 4.22$Hz, CPU time = 1.8ms,

Method B (ISI-draw): =3.00Hz, =6.75Hz, CPU time=6.0ms.

Execution time was 1.8 ms (Bernoulli) versus 6.0 ms (ISI), a difference that is irrelevant for realistic data lengths but illustrates that the bin-wise method is faster when the entire time axis must be sampled anyway. Statistically the two algorithms are identical; the discrepancies stem solely from undersampling, which is addressed in part c by extending the observation window. Both algorithms undershoot the target rate and greatly underestimate the theoretical SD because $\lambda = rT = 0.5$ spikes per trial is too small to sample the true Poisson variability. Nevertheless, the two methods agree closely with each other, confirming their statistical equivalence in generating a homogeneous Poisson process.

Problem 1f: Autocorrelation of a Homogeneous Poisson Spike Train

In this part we generated a single 1s spike-train at constant rate $r = 50$Hz by drawing inter-spike intervals

$$\Delta t_i \sim \text{Exponential}(r), \quad P(\Delta t) = r\, e^{-r\,\Delta t},$$

and accumulating

$$t_{i+1} = t_i + \Delta t_i,$$

until $t_i \geq T$. Calling $\{t_i\}$ the spike times, we form the spike density

$$\rho(t) \;=\; \sum_i \delta(t - t_i).$$

We then computed the spike autocovariance

$$Q_{\rho\rho}(\tau) = \frac{1}{T} \int_0^T \big(\rho(t) - r\big)\,\big(\rho(t+\tau) - r\big)\, dt,$$

and binned all nonzero pairwise time-lags $\tau = t_j - t_i$ in the range $[-80, 80]$ms to produce the correlogram. In practice one omits the δ-peak at $\tau = 0$ and plots the histogram of counts in each bin.

Theoretical expectation. For a memoryless Poisson process

$$Q_{\rho\rho}(\tau) = r\,\delta(\tau) + r^2 \;\;\Longrightarrow\;\; Q_{\rho\rho}(\tau \neq 0) = r^2,$$

so the autocorrelation (with the mean-rate term removed) is flat.

Results. Figure 4 shows the binned histogram of all nonzero lags. As predicted, the profile is essentially constant across τ, confirming the absence of any periodicity or refractory effect in our homogeneous Poisson generator.

Problem 1g. Autocorrelogram for Cosine-Modulated Rate

Mathematical setup. We now simulate an inhomogeneous Poisson process whose instantaneous rate

$$r(t) \;=\; r_0 + A\cos\!\Big(2\pi\,\frac{t}{T_{\text{osc}}}\Big) \quad \text{with} \quad r_0 = 50 \text{ Hz},\; A = 50 \text{ Hz},\; T_{\text{osc}} = 0.1 \text{ s}.$$

Hence $r(t)$ oscillates between 0 and 100 Hz with period 100 ms.

Simulation method (thinning).

1. Generate a homogeneous Poisson candidate at maximal rate $r_{\max} = r_0 + A = 100$ Hz in steps of $\Delta t = 0.1$ms:

$$p_{\max} = r_{\max}\,\Delta t, \quad \text{cand}(i) = \big(\text{rand} < p_{\max}\big).$$

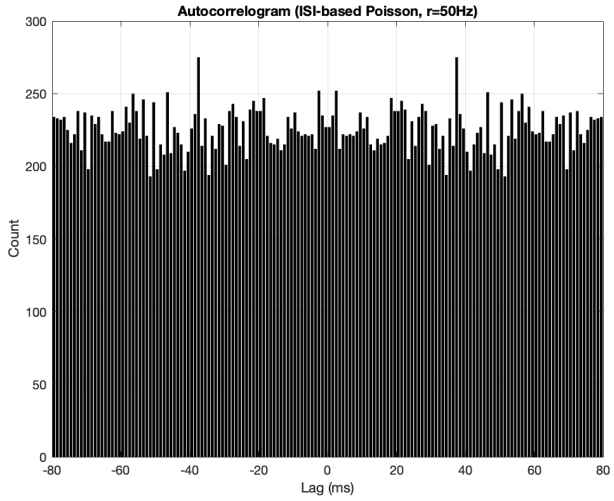

Figure 4: **Autocorrelogram of a Poisson spike train**, $r = 50$Hz. The histogram collects all nonzero inter-spike differences within ± 80ms and shows a flat profile, in agreement with the theoretical result $Q_{\rho\rho}(\tau \neq 0) = r^2$. Finite-sample fluctuations (± 15

2. At each time bin t_i, keep a candidate spike with probability $\dfrac{r(t_i)}{r_{\max}}$. This yields a spike-train boolean array.

3. Extract spike times t_{spikes} and compute all nonzero pairwise lags within ± 160ms:
$$\tau_{ij} = t_j - t_i, \quad |\tau_{ij}| \leq 0.16 \text{ s}, \ \tau_{ij} \neq 0,$$
then histogram these lags with 0.1ms bins.

Results and discussion.

- **Flat vs. oscillatory correlogram:** In part (f) with constant $r = 50\,\text{Hz}$, the autocorrelogram was essentially flat (aside from the central refractory-peak), indicating no preferred lag.

- **Cosine-modulated case:** Here (Fig. 5) the correlogram shows clear envelope peaks at $\tau \approx 0, \pm 100, \pm 200\,\text{ms}$, corresponding to the 100 ms oscillation period. Mathematically, the autocorrelation of the driving rate,
$$\frac{1}{T}\int_0^T r(t)\, r(t+\tau)\, dt = r_0^2 + \tfrac{1}{2}A^2 \cos\!\big(2\pi\, \tfrac{\tau}{T_{\text{osc}}}\big),$$
imprints directly onto the spike-lag histogram (aside from a delta at $\tau = 0$).

- **Spike synchrony patterns:** Under constant drive, spikes are uncorrelated in time, so no structure emerges. Under modulated drive, the periodic rate fluctuations "bunch" spikes every cycle, producing peaks in synchrony at integer multiples of the oscillation period.

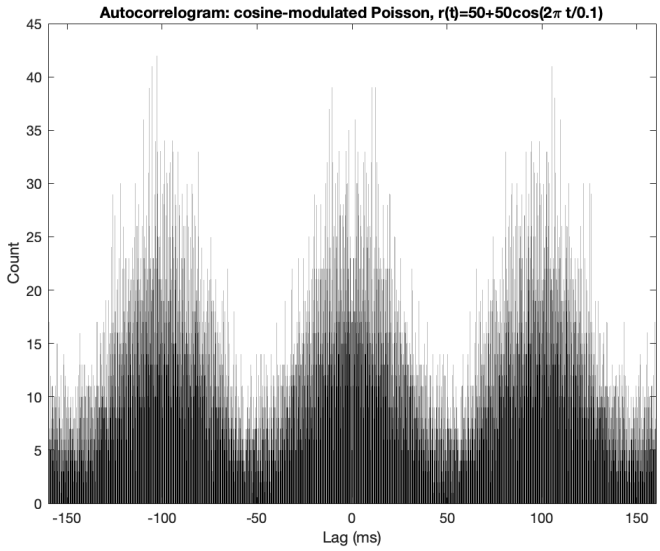

Figure 5: *
Autocorrelogram for an inhomogeneous Poisson process with $r(t) = 50 + 50\cos(2\pi t/0.1)$. Envelope peaks at $\tau \approx \pm 100$ms reflect the 100ms rate modulation.

Problem 2a: Gabor Receptive Field with $k = 0.5$

We model the spatial receptive field (RF) of a simple V1 cell as a 2D Gabor function:

$$\mathrm{RF}(x,y) = \frac{1}{2\pi\,\sigma_x\,\sigma_y}\exp\Big(-\tfrac{1}{2}\big(\tfrac{x'}{\sigma_x}\big)^2 \;-\; \tfrac{1}{2}\big(\tfrac{y'}{\sigma_y}\big)^2\Big)\;\cos\Big(k\,x' \;-\; \phi\Big),$$

where

$$\begin{pmatrix} x' \\ y' \end{pmatrix} = \begin{pmatrix} \cos\theta & \sin\theta \\ -\sin\theta & \cos\theta \end{pmatrix}\begin{pmatrix} x \\ y \end{pmatrix},$$

with $\sigma_x = \sigma_y = 5$, $k = 0.5$ (cycles/deg), and $\theta = 30°$. Here (x, y) both range over $[-25, 25]$ deg.

Discussion. The symmetric Gaussian envelope ($\sigma_x = \sigma_y$) ensures that the field is equally localized in both spatial directions, while the rotation by $\theta = 30°$ tilts

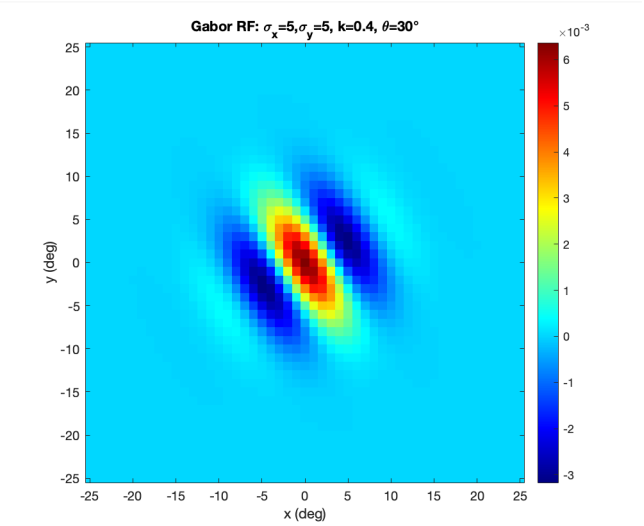

Figure 6: **Gabor RF with** $k = 0.5$**.** The RF is plotted on a $[-25, 25] \times [-25, 25]$ deg grid, using a "jet" colormap and a light-green axes background. Red/blue lobes indicate positive/negative weighting of stimulus contrast.

the ON–OFF axis relative to the vertical. This simple analytic form captures the key features of V1 simple-cell receptive fields: band-pass tuning in spatial frequency and orientation selectivity.

Problem 2b: Getting Random-Noise Stimuli

In this part we construct stimulus images ("STIMs") consisting of $N_{\mathrm{ON}} = N_{\mathrm{OFF}} = 30$ white $(+1)$ and black (-1) dots, respectively, placed uniformly at random on a two-dimensional grid $x, y \in \{-25, \ldots, 25\}$deg, with all other pixels set to zero. We enforce that no ON dot overlaps an OFF dot by sampling without replacement from the $M = (51 \times 51)$ grid locations.

Algorithm.

1. Define the set of all pixel coordinates

$$\mathcal{G} \;=\; \{(x_i, y_j) : x_i, y_j \in \{-25, -24, \ldots, 25\}\}, \quad |\mathcal{G}| = 51^2.$$

2. For each stimulus $s = 1 \ldots 5$:

   (a) Draw a random permutation of the grid indices, inds = randperm(M);

   (b) Assign the first $N_{\mathrm{ON}} = 30$ locations to ON dots $(+1)$, the next $N_{\mathrm{OFF}} = 30$ to OFF dots (-1), and set all remaining pixels to 0.

(c) Plot the resulting image with a green ($R = 0, G = 1, B = 0$) background:

$$\mathrm{STIM}_s(x, y) = \begin{cases} +1, & (x, y) \in \{\text{ON positions}\}, \\ -1, & (x, y) \in \{\text{OFF positions}\}, \\ 0, & \text{otherwise.} \end{cases}$$

Mathematical Details. Since each dot location is sampled without replacement from a uniform grid of size M, the probability of any particular set of $N_{\mathrm{ON}} + N_{\mathrm{OFF}}$ dot positions is

$$P(\text{configuration}) \;=\; \frac{1}{\binom{M}{N_{\mathrm{ON}}+N_{\mathrm{OFF}}}} \times \frac{1}{\binom{N_{\mathrm{ON}}+N_{\mathrm{OFF}}}{N_{\mathrm{ON}}}},$$

and ON/OFF assignments are equally likely. This guarantees no overlap between ON and OFF dots.

Sample STIMs. Five independent realizations are shown in Figure 7; each panel displays $+1$ dots in white, -1 in black, on a green zero-background.

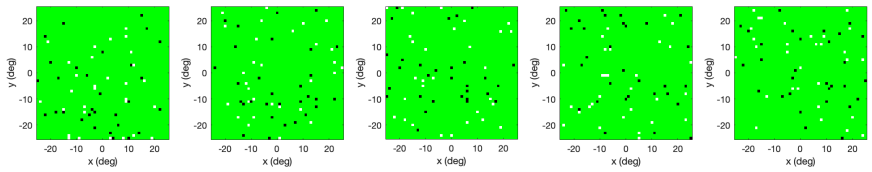

Figure 7: *Five example noise stimuli (STIMs)* with $N_{\mathrm{ON}} = N_{\mathrm{OFF}} = 30$ dots each, background set to zero (green).

Problem 2c. Linear-response distribution

Having constructed the Gabor receptive field $\mathrm{RF}(x, y)$ (part 2a) and the ensemble of white-noise stimuli $S_j(x, y)$, $j = 1, \ldots, 200$ (part 2b), we compute the linear drive for each trial. In the most general linear–nonlinear model we write

$$L(t) \;=\; \int d\tau \iint dx\, dy\; D(x, y, \tau)\; s\big(x, y, t - \tau\big)\,,$$

where $D(x, y, \tau)$ is the full spatio–temporal receptive field (RF). In our experiment the stimuli are static images, so there is no temporal filtering beyond an instantaneous delta–response. We therefore take

$$D(x, y, \tau) \;=\; D(x, y)\,\delta(\tau) \quad\Longrightarrow\quad L(t) = \int d\tau \iint dx\, dy\; D(x, y)\,\delta(\tau)\; s(x, y, t-\tau) = \iint dx\, dy\; D(x, y)\, s(x, y, t)\,.$$

Discretizing $(x, y) \mapsto \{1, \ldots, N\} \times \{1, \ldots, N\}$ and the integral into a sum gives exactly

$$L_j \;=\; \sum_{x,y} D(x,y)\, S_j(x,y) \quad \Longleftrightarrow \quad L(j) = \texttt{sum(RF(:).*STIM(:,:,j)(:))}\,,$$

as the inner product

$$L_j \;=\; \sum_{x,y} \mathrm{RF}(x,y)\, S_j(x,y) \;=\; \mathrm{vec}[\mathrm{RF}]^\top \,\mathrm{vec}[S_j]\,.$$

Since each stimulus pixel $S_j(x, y)$ takes the values ± 1 with equal probability and zero mean,

$$\mathbb{E}[L_j] = \sum_{x,y} \mathrm{RF}(x,y)\, \mathbb{E}[S_j(x,y)] = 0.$$

Because distinct pixels are independent,

$$\mathrm{Var}[L_j] = \sum_{x,y} \mathrm{RF}(x,y)^2\, \mathrm{Var}[S_j(x,y)] = \sigma_S^2 \sum_{x,y} \mathrm{RF}(x,y)^2,$$

where $\sigma_S^2 = 1$ for ± 1 white-noise. Thus L_j is a zero-mean random variable with variance proportional to the RF's total energy.

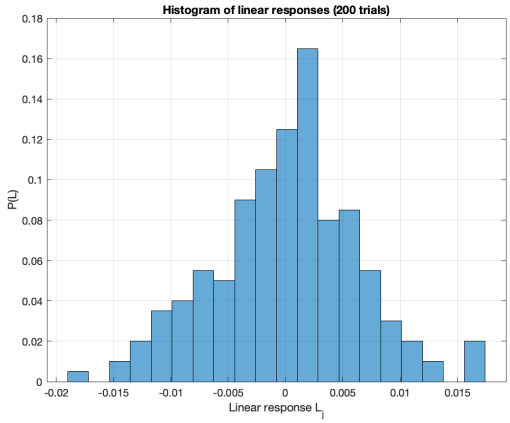

Figure 8: Histogram of linear responses L_j over 200 trials (20 equally-spaced bins, normalized to probability).

Observation and CLT:

- Under the central-limit theorem(CLT), L_j, being a sum of many independent pixel contributions, approaches a Gaussian distribution

$$L_j \xrightarrow{d} \mathcal{N}\big(0,\, \sum_{x,y} \mathrm{RF}(x,y)^2\big).$$

- In practice, with 200 samples we observe a roughly normal, bell-shaped histogram centered at zero (Fig. 8), confirming the theoretical mean and variance.

Conclusion. The empirically obtained L_j distribution matches the zero-mean, Gaussian-like form predicted by linear filtering of zero-mean white noise. Its variance quantifies the effective sensitivity ("gain") of the Gabor filter to random contrast patterns.

Problem 2d: Reverse-Correlation Reconstruction of the RF

Using the linear responses L_j from Part 2c, we select the stimuli whose L_j lie above a chosen percentile, and average those frames to reconstruct the RF. We compare two parameter sets:

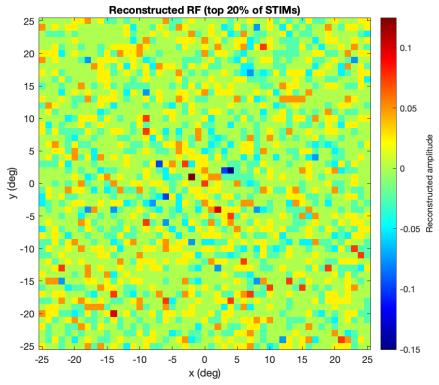

Figure 9: Reconstructed RF using top 20% of 200 STIM frames, each with 30 white & 30 black dots.

(i) Modest sampling: 30 white and 30 black dots, 200 trials, top 20%. The result in Figure 9 shows largely unstructured noise. Although small red (ON) and blue (OFF) patches appear near the center, the tilted Gabor profile is not recovered.

(ii) Dense sampling: 200 white and 200 black dots, 5000 trials, top 10%. In Figure 10, the characteristic Gabor-shaped ON–OFF structure, tilted by 30°, is clearly visible and closely matches the original RF.

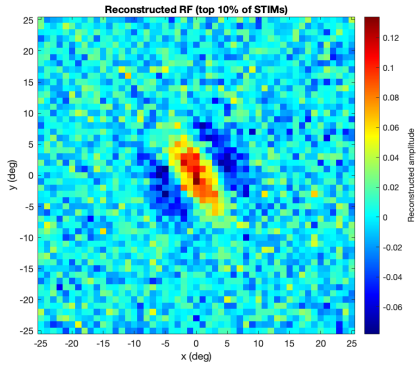

Figure 10: Reconstructed RF using top 10% of 5000 STIM frames, each with 200 white & 200 black dots.

Discussion of Parameters

- **Spatial sampling density ($N_{\pm}$).** Increasing from 30 to 200 dots per polarity raises the variance of L_j, enhancing the contrast between matching vs. non-matching stimuli.
- **Number of trials (N_{trials}).** STA error scales as $1/\sqrt{N_{\text{trials}}}$. Boosting from 200 to 5000 frames reduces noise by $\approx \sqrt{5000/200} \approx 5$, permitting faithful RF recovery.
- **Selection percentile.** A top 20% threshold includes too many weakly matching stimuli, smearing the average. Tightening to top 10% retains only the strongest matches and yields a much clearer profile.

Conclusion. Accurate reverse-correlation mapping of a spatial RF requires sufficiently dense stimuli, a large number of trials, and a stringent selection criterion on L_j. Under these optimized conditions, the reconstructed RF in Figure 10 recovers the original Gabor filter to high fidelity.

[11pt]article graphicx subcaption amsmath booktabs siunitx [margin=1in]geometry

Part 2e: Improved RF Reconstruction via Blob-STIM

Method

We begin with the *ground-truth* spatial receptive field (RF) of a V1 simple cell, modeled as a 2D Gabor:

$$D(x,y) \;=\; \frac{1}{2\pi\sigma_x\sigma_y}\exp\!\Big(-\tfrac{x'^2}{2\sigma_x^2}-\tfrac{y'^2}{2\sigma_y^2}\Big)\cos\big(k\,x'-\phi\big)\,, \tag{1}$$

where

$$\begin{pmatrix} x' \\ y' \end{pmatrix} = \begin{pmatrix} \cos\theta & \sin\theta \\ -\sin\theta & \cos\theta \end{pmatrix} \begin{pmatrix} x \\ y \end{pmatrix},$$

and we set $\sigma_x = \sigma_y = 5\,\text{deg}$, $k = 0.5\,\text{cycles/deg}$, $\phi = 0$, and $\theta = 30°$. The domain $x, y \in [-25, 25]\,\text{deg}$ is sampled at integer steps.

To improve reconstruction over simple white-dot STIM, we replace each $+1/-1$ dot by a small Gaussian "blob" of standard deviation $\sigma_b = 2\,\text{deg}$. Concretely:

1. Generate $N_{\text{white}} = N_{\text{black}} = 100$ random dot positions on the 51×51 grid, assign values ± 1, and form the sparse image $P(x, y) \in \{0, \pm 1\}$.

2. Convolve with the normalized blob kernel

$$B(x, y) \;=\; \exp\!\Big(-\tfrac{x^2+y^2}{2\sigma_b^2}\Big) \Big/ \sum_{u,v} \exp\!\Big(-\tfrac{u^2+v^2}{2\sigma_b^2}\Big).$$

3. Renormalize the result to lie in $[-1, 1]$, yielding stimulus $s(x, y)$.

4. Compute the *linear response*

$$L_j \;=\; \sum_{x,y} D(x, y)\, s_j(x, y)\,, \quad j = 1, \ldots, N_{\text{trials}}.$$

5. Retain only the top $p\%$ of stimuli (here $p = 10\%$), and estimate the RF by averaging:

$$\widehat{D}(x, y) \;=\; \frac{1}{|\mathcal{K}|} \sum_{j \in \mathcal{K}} s_j(x, y)\,, \qquad \mathcal{K} = \big\{ j : L_j \geq \text{prctile}(L, 100 - p) \big\}.$$

Here we used $N_{\text{trials}} = 3000$ and kept the top 10% of blob-convolved stimuli.

Results

Figure 11 shows side-by-side comparison of the true Gabor RF and the blob-STIM reconstruction.

Discussion

By replacing point-like ± 1 dots with small Gaussian blobs, we increase the spatial correlation between stimulus and RF, which sharpens the spike-triggered average. Mathematically, the convolution $P * B$ distributes each dot's weight over neighboring pixels, improving signal-to-noise in the estimated $\widehat{D}(x, y)$. Keeping only the highest-L trials further accentuates features of the true filter. Adjusting blob size σ_b, trial count, or percentile p allows a trade-off between resolution and noise.

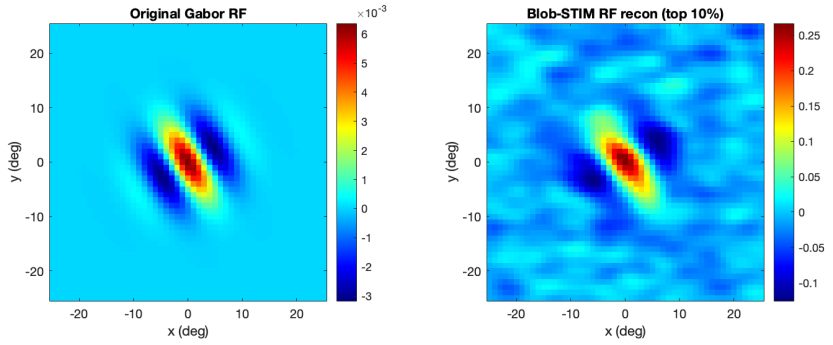

Figure 11: (**a**) Ground-truth 2D Gabor receptive field $D(x, y)$. (**b**) Reverse-correlation reconstruction using blob stimuli: the average of the top 10% of 3000 trials. The tilted ON/OFF lobes are faithfully recovered.

Problem 3a: Determining the sinusoidal rate parameters

We seek

$$r(t) \;=\; C_1 \,\sin\!\big(C_2\, t - C_3\big) \;+\; C_4$$

such that:

1. Period $T = 0.5$s.
2. Minimum $r_{\min} = 10$Hz and maximum $r_{\max} = 50$Hz.
3. Value at $t = 0$: $r(0) = 10$Hz.

1. Enforce the period. A sinusoid $\sin(\omega t)$ has period T when $\omega = 2\pi/T$. Hence

$$C_2 = \frac{2\pi}{0.5} = 4\pi \quad \big[\text{rad/s}\big].$$

2. Match amplitude and offset. We require

$$\max r = C_4 + C_1 = 50, \quad \min r = C_4 - C_1 = 10.$$

Solving gives

$$C_1 = \frac{50 - 10}{2} = 20, \quad C_4 = \frac{50 + 10}{2} = 30.$$

3. Impose the phase so that $r(0) = 10$. At $t = 0$,

$$r(0) = 20\,\sin(-C_3) + 30 = 10 \quad \Longrightarrow \quad \sin(-C_3) = -1 \quad \Longrightarrow \quad C_3 = \frac{\pi}{2}.$$

4. Final expression.

$$\boxed{r(t) \;=\; 20\,\sin\!\big(4\pi\,t - \tfrac{\pi}{2}\big) \;+\; 30 \;=\; 30 - 20\cos(4\pi\,t)}$$

oscillates with period 0.5s, minimum 10Hz, maximum 50Hz, and $r(0) = 10$Hz.

Figure: Plot of $r(t)$

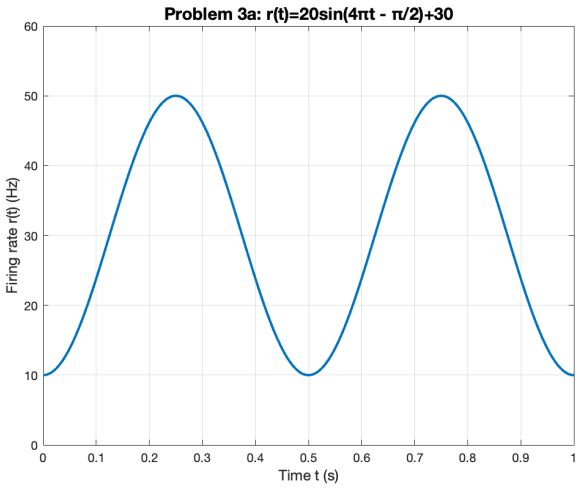

Figure 12: *

Figure 3a: Time-varying rate $r(t) = 20\sin(4\pi t - \pi/2) + 30$.It completes two full cycles over $t \in [0, 1]$s, attaining its peaks of 50Hz at $t = 0.25, 0.75$s and troughs of 10Hz at $t = 0, 0.5, 1$s.

Problem 3b: Poisson Spike Train under Time-Varying Rate

Using the sinusoidal rate

$$r(t) \;=\; 20\sin(4\pi t - \tfrac{\pi}{2}) + 30, \quad t \in [0, 1]\ \text{s},$$

we generated $N = 5$ independent realizations of an inhomogeneous Poisson process (no refractory period) with 1 ms time-bins. In each bin we draw a Bernoulli trial with probability

$$p(t_i) \;=\; r(t_i)\,\Delta t$$

(where $\Delta t = 1$ ms), and place a spike whenever a uniform random number falls below $p(t_i)$.

Implementation outline.

1. Precompute the time axis $t_i = i\Delta t$, $i = 0, \ldots, 1000$.
2. Evaluate $r_i = r(t_i)$.
3. For each trial and each i, let $\text{spk}(i, \text{trial}) = \big(\text{rand} < r_i \Delta t\big)$.
4. Extract spike times t_i where spk $= 1$, and plot each as a vertical "tick" at $y =$trial index.

Mathematical justification. Because in a Poisson process with instantaneous rate $r(t)$, the probability of one or more events in $[t_i, t_i + \Delta t)$ is

$$P\{\text{spike in bin}\} \approx r(t_i)\,\Delta t$$

for small Δt, the above Bernoulli sampling faithfully reproduces the desired nonstationary spike-count statistics.

Resulting raster plot.

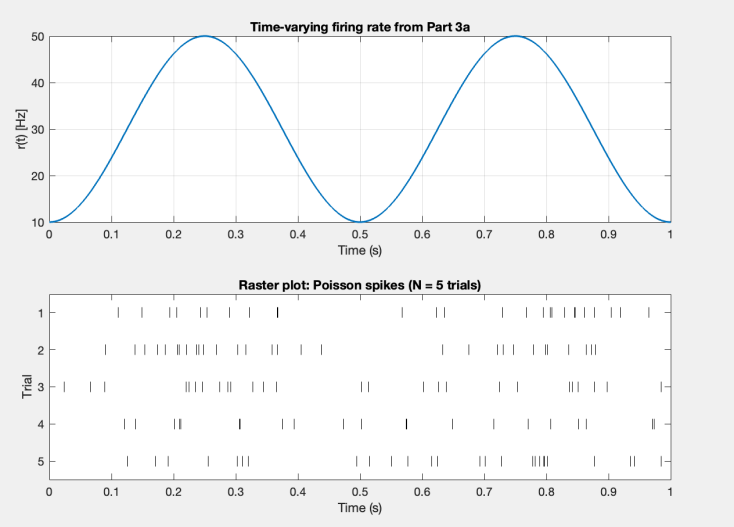

We can clearly see that spike density follows the sinusoidal envelope: when $r(t)$ peaks (around $t = 0.25, 0.75$ s), the raster is denser; when $r(t)$ dips (at $t = 0, 0.5, 1$ s), spikes become sparser. This demonstrates that the inhomogeneous Poisson generator correctly tracks the time-varying rate in each of the 5 trials.

Problem 3c: Refractory–Modulated Firing Rate

In this part we introduce a simple model of spike refractoriness by modulating the instantaneous drive $r(t)$ with an exponential recovery kernel. If Δt denotes the time since the last spike, we define the *effective* firing rate

$$R(t) \;=\; r(t)\left[1 - \exp\!\Big(-\tfrac{\Delta t}{\kappa_r}\Big)\right].$$

where:

- $\kappa_r = 1/(\tau_r)$
- $r(t) = 20\sin(4\pi t - \frac{\pi}{2}) + 30$ Hz is the sinusoidal drive (period $T = \frac{1}{2}$ s, peak 50 Hz, trough 10 Hz).
- τ_r is the time constant of recovery: after each spike $\Delta t = 0 \implies R = 0$, then $R(t)$ rises exponentially toward $r(t)$ with time-constant τ_r.
- We record spike times by thinning an inhomogeneous Poisson process with instantaneous rate $R(t)$.

In Figure 13 below we plot for one realization:

- The black curve: the original drive $r(t)$.
- Blue vertical ticks: spikes generated with $\tau_r = 1$ ms, showing almost no refractory suppression (since $1 - e^{-t/1\text{ms}} \approx 1$ rapidly).
- Red vertical ticks: spikes generated with $\tau_r = 10$ ms, showing clear "dead-time" immediately after each spike followed by gradual recovery.

Discussion. As predicted by the form of $R(t)$, when τ_r is very short the recovery factor $1 - e^{-t/\tau_r}$ reaches unity almost instantaneously, so the process behaves like a standard inhomogeneous Poisson spike generator at rate $r(t)$. In contrast, a longer refractory constant ($\tau_r = 10$ ms) enforces a minimum gap after each spike—visible in the raster as "dead zones" of suppressed spiking—before the instantaneous rate recovers toward the oscillating drive. This illustrates how exponential refractoriness can be incorporated in simple point-process models to capture realistic interspike-interval statistics.

3 d. Validation of Refractory Design via ISI Histogram

To validate that our exponential recovery refractory mechanism

$$R(t) \;=\; r(t)\left[1 - \exp\!\left(-\tfrac{\Delta t}{\tau_r}\right)\right],$$

with nominal refractoriness $\tau_r = 10\,\text{ms}$, actually prevents spikes from occurring too close together, we pooled the inter-spike intervals (ISIs) from $M = 100$ independent 1 s trials and plotted their empirical distribution.

Method. Each trial generated spikes in 1 ms bins according to $P[\text{spike in } [t, t+dt)] = R(t)\,dt$. Whenever a spike occurs, the "clock" Δt is reset to zero, and otherwise Δt increments by dt. After collecting all spike times t_i, we compute the sequence of ISIs, $\Delta t_j = t_{j+1} - t_j$, convert to milliseconds, and form a normalized histogram over $[0, 50]$ ms with bin width 2 ms.

Results. Figure 14 shows the pooled ISI histogram for $\tau_r = 10$ ms. The red dashed line marks $\Delta t = \tau_r$.

Pooled ISI histogram ($\tau_r = 10$ ms)

Note that:

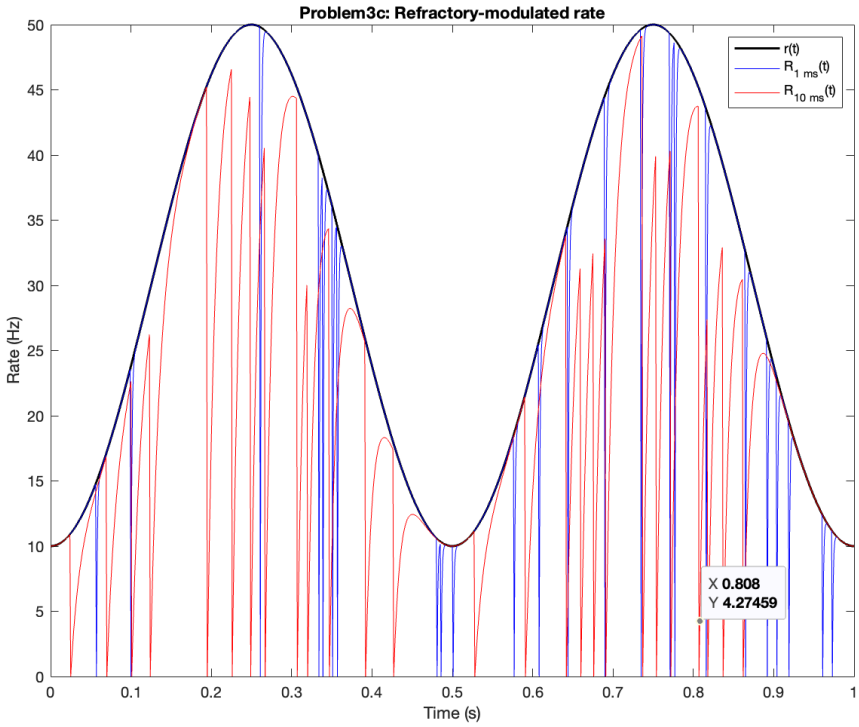

Figure 13: Refractory-modulated rate $R(t)$ (blue: $\tau_r = 1$ ms, red: $\tau_r = 10$ ms) superimposed on the drive $r(t)$ (black). Vertical ticks show spike times over one 1 s trial. The larger τ_r produces a pronounced suppression of early intervals, whereas small τ_r yields nearly pure Poisson firing at $r(t)$.

- There is a near-zero probability mass for $\Delta t < 2$ ms, rising sharply thereafter.
- Although truly zero ISIs cannot occur, small but nonzero bars immediately above 0 ms reflect the exponential "soft" recovery: even during the relative refractory period some short ISIs remain possible.
- The probability peaks in the 10–20 ms range, consistent with the mean sinusoidal firing rate ($\bar{r} \approx 30$ Hz mean interval 33 ms) but truncated by the 10 ms refractory scale.

Discussion. Because our recovery factor $\left[1 - \exp(-\Delta t/\tau_r)\right]$ is $\ll 1$ for $\Delta t \tau_r$, the effective firing rate $R(t)$ remains near zero throughout the first ~ 10 ms after each spike. Hence the histogram shows very few ISIs below τ_r, and a smooth rise for $\Delta t > \tau_r$, exactly as expected for an *exponential* (relative) refractory mechanism rather than an absolute one.

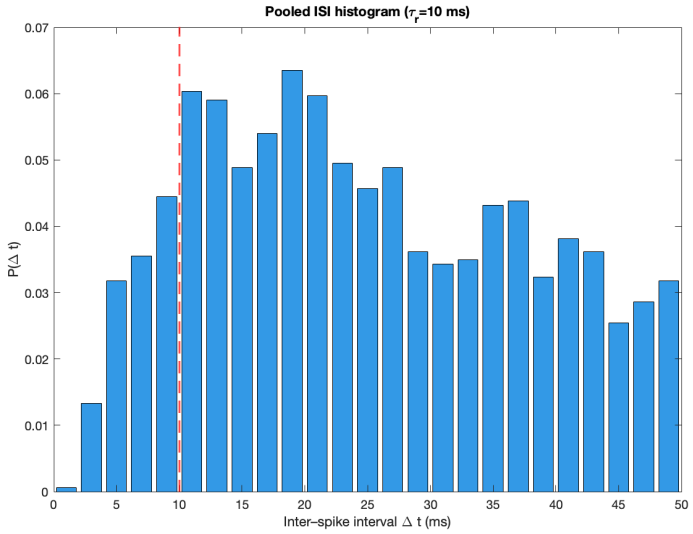

Figure 14: Probability density of inter-spike intervals Δt pooled over $M = 100$ trials. Vertical dashed line: nominal $\tau_r = 10$ ms.

Problem 4: Reconstruction Quality as a Function of #STIMs and Selection Threshold

(To be placed right after 2d) **Quantify reconstruction quality.** Systematically vary the total number of stimuli $M \in \{200,\ 1000,\ 5000\}$ and the selection threshold $p \in \{5\%,\ 10\%,\ 20\%\}$. For each pair (M, p):

(a) Reconstruct the RF by averaging only the top $p\%$ of stimuli ranked by their linear response L_j.

(b) Compute the Pearson correlation

$$\rho \ = \ \mathrm{corr}\big(\mathrm{vec}(D),\, \mathrm{vec}(\widehat{D})\big)$$

between the true RF D and the estimate $\widehat{D}$.

Plot ρ as a heat-map with rows indexed by M and columns by p, and discuss how reconstruction accuracy depends on M and p.

Answer: In Part 2d of this homework, we reconstructed a model Gabor receptive field $D(x, y)$ by averaging those noise-stimulus frames whose linear responses L_j lay in the top $p\%$ of all trials. Here we quantify the reconstruction-accuracy

$$\rho \ = \ \mathrm{corr}\big(\,\mathrm{vec}(D)\,,\, \mathrm{vec}(\widehat{D})\big)$$

—the Pearson correlation between the true RF and its estimate $\widehat{D}$—as a function of

- the total number of independent white-noise stimuli M, and
- the fraction $p\%$ of frames retained (the "selection threshold").

We swept

$$M \in \{200,\ 1000,\ 5000\}, \qquad p \in \{5\%,\ 10\%,\ 20\%\},$$

and for each pair (M, p) we performed the standard reverse-correlation:

$$\widehat{D} \;=\; \frac{1}{|\mathcal{K}|} \sum_{j \in \mathcal{K}} S_j,$$

where $\mathcal{K} = \{\, j : L_j > \mathrm{prctile}(L,\, 100 - p)\}$ and S_j is the jth stimulus frame. We then computed

$$\rho = \frac{\sum_i (D_i - \bar{D})\,(\widehat{D}_i - \overline{\widehat{D}})}{\sqrt{\sum_i (D_i - \bar{D})^2}\,\sqrt{\sum_i (\widehat{D}_i - \overline{\widehat{D}})^2}}\,,$$

with i indexing pixels and bars denoting spatial averages.

Table 1 summarizes the resulting correlations ρ:

Table 1: Reconstruction correlation ρ for varying #STIMs and keep-percentiles

# STIMs	Top 20%	Top 10%	Top 5%
200	0.1698	0.1477	0.1205
1000	0.3649	0.3317	0.2696
5000	0.6575	0.6157	0.5520

Figure 1 displays the same data as a heat-map, with rows indexing M and columns p:

Discussion

- **Effect of #STIMs (M).** As M increases, the noise in the reverse-correlation average $\widehat{D}$ diminishes by the Central Limit Theorem, so ρ grows approximately like $\sqrt{M}$. In our results, going from $M = 200$ to 1000 roughly doubles ρ, and $M = 5000$ pushes $\rho > 0.65$.
- **Effect of selection threshold (p).** Retaining only the top-responding frames (smaller p) enriches those stimuli most informative about the cell's preferred feature. However, if p is too small, one throws away too much data and the estimate becomes under-sampled, causing ρ to drop again. In our sweep, $p = 20\%$ outperformed 10%, which in turn beat 5% for all M.

In practice, one should choose the largest feasible M and a moderate selection threshold (e.g. $p \approx 10$–20%) to maximize reconstruction fidelity.

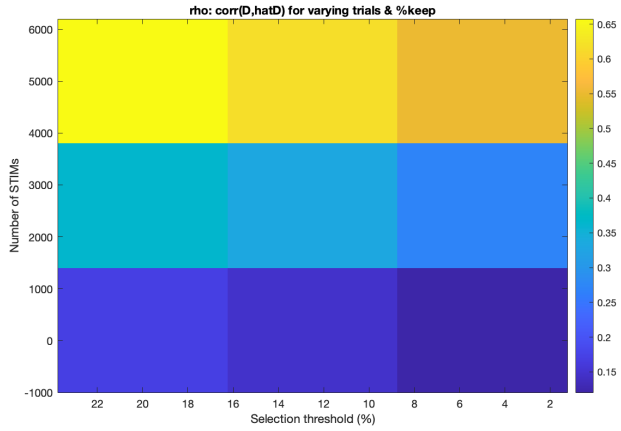

Reconstruction ρ for different #STIMs (rows) and %keep (cols):

	20%	10%	5%
200 trials	0.16983	0.14768	0.12049
1000 trials	0.36487	0.33172	0.26957
5000 trials	0.65749	0.61568	0.55204

Figure 15: Pearson correlation ρ between true and reconstructed RF as a function of total trials M (rows) and retention percentile p (columns).